

# Learning ECG Representations based on Manipulated Temporal-Spatial Reverse Detection

Wenrui Zhang<sup>a</sup>, Shijia Geng<sup>b</sup>, Shenda Hong<sup>c,d,\*</sup>

<sup>a</sup>*Department of Mathematics, National University of Singapore, Singapore, 119077, Singapore*

<sup>b</sup>*HeartVoice Medical Technology, Hefei, 230027, China*

<sup>c</sup>*National Institute of Health Data Science at Peking University, Peking University, Beijing, 100191, China*

<sup>d</sup>*Institute of Medical Technology, Health Science Center of Peking University, Beijing, 100191, China*

---

## Abstract

Learning representations from electrocardiogram (ECG) serves as a fundamental step for many downstream machine learning-based ECG analysis tasks. However, the learning process is always restricted by lack of high-quality labeled data in reality. Existing methods addressing data deficiency either cannot provide satisfied representations for downstream tasks or require too much effort to construct similar and dissimilar pairs to learn informative representations. In this paper, we propose a straightforward but effective approach to learn ECG representations. Inspired by the temporal and spatial characteristics of ECG, we flip the original signals horizontally, vertically, and both horizontally and vertically. The learning is then done by classifying the four types of signals including the original one. To verify the effectiveness of the proposed temporal-spatial (T-S) reverse detection method, we conduct a downstream task to detect atrial fibrillation (AF) which is one of the most common ECG tasks. The results show that the ECG representations learned with our method lead to remarkable performances on the downstream task. In addition, after exploring the representational feature space and investigating which parts of the ECG signal contribute to the representations, we conclude that the temporal reverse is more effective than the spatial reverse for learning ECG representations.

*Keywords:* deep learning, representation learning, Electrocardiogram

---

## 1. Introduction

People used to design specific machine learning models for specific tasks. However, with accumulated experience in deep learning, they have uncovered that models trained for certain tasks with sufficient data can facilitate the training of other tasks requiring similar data [1]. Two-stage deep learning frameworks then emerge and become prevailing [2, 3]. The first stage always refers to the pre-training stage where models are trained to perform general tasks using a large amount of labeled data. After training, models are able to generate “representations” [4, 5] that contain information based on the models’ understandings of data gained from learning to perform the general tasks. Such representations can then be used for the actual tasks in the second stage which are often called the downstream tasks.

As deep learning becomes the popular tool for specific electrocardiogram (ECG) tasks [6] such as disease detection [7, 8, 9, 10], sleep staging [11, 12], biometric human identification [13, 14], and denoising [15], people start considering learning general representations of ECG using pre-training models [16, 17, 18, 19].

However, high-quality labeled data is difficult to acquire, especially in the medical area. Actually, two types<sup>1</sup> of methods have already been developed to tackle the problem, and the details are as follows:

---

\*Corresponding author.

*Email address:* hongshenda@pku.edu.cn (Shenda Hong)

<sup>1</sup>We do not categorize the methods based on unsupervised learning or self-supervised learning since there are overlaps between the two learning concepts.

- **Reconstruction:** this type of approaches tries to reserve as much information of the original data as possible, and does not require any label of data. It learns from data structure and reduces the dimension of data through removing the redundancy of data with methods such as principal component analysis [20] (PCA) and autoencoder [21] (AE). These methods are widely employed in dimension reduction of ECG data [22, 23, 24]. Although they are easy to implement, the performance of downstream tasks with representations learned from these methods are usually unsatisfactory.
- **Contrastive learning (CL):** CL methods have drawn much attention in recent years, and have been applied in learning representation from ECG as well [16, 17, 18, 19]. CL attempts to design the “pretext task” to learn representation from unlabeled data which is prior to and will facilitate the downstream training for the actual task. In detail, it constructs positive pairs and negative pairs by domain knowledge or data augmentation. Then, model is trained by maximizing the similarity of positive pairs and minimizing the similarity of negative pairs. CL provides a way to discover the supervised information from unlabeled data, and trains the model similar to supervised learning. The representations learned from CL show greater performance on downstream tasks. However, the framework of CL is sophisticated and constructing training pairs is difficult and sometimes even not possible.

To address the problems of the above methods, we aim to design a supervised-like pre-training task with unlabeled data. Our method can provide effective representations for ECG downstream tasks while avoiding spending time and effort on constructing negative and positive pairs. Inspired by the temporal and spatial characteristics of ECG signals, in this paper, we propose a straightforward but remarkably effective representation learning method by detecting simply manipulated ECG signals from the original ones. In detail, we first divide the original signals into segments and manipulate the segments with three easy transformations: flipping horizontally (corresponding to temporal characteristics), vertically (corresponding to spatial characteristics), and both horizontally and vertically (corresponding to both). We then train the representational model by classifying these four classes of ECG segments. After pre-training, the model is transferred to the downstream task. Moreover, we use an interpretation method to understand the possible explanations behind our method.

We conduct atrial fibrillation (AF) detection as the downstream task to evaluate our learned representations. The experimental results show that our simply implemented pre-training task outperforms other baseline methods by a large margin. From the results, we also observe that the detection of temporal reverse helps learn better representations than spatial reverse detection. The interpretation results indicate that the detection of spatial reverse can be easily achieved by observing peaks of ECG signals, and thus the representations contain less information. On the other hand, detecting temporal reverse needs to consider more points from the ECG signals, so the representations contain more information.

## 2. Materials and methods

### 2.1. Dataset

We use the publicly available and widely used dataset from PhysioNet Computing in Cardiology Challenge 2017 (CinC 2017) [25]. The data is collected and band-pass filtered by AliveCor device. The sampling rate of all ECG signals is 300 Hz, and the time length ranges from 9 s to over 60 s. The whole training set contains 8,528 single-lead ECG recordings. There are five classes of ECG signals in this dataset, and we only select ECG signals with “normal” and “AF” labels. An overview of the data we choose is shown in Table 1.

We perform data preprocessing following two steps: (1) we split all recordings into 10-second segments using sliding window with 5-second stride. The segments that are shorter than 3000 (10 s  $\times$  300 Hz) are discarded. (2) we normalize each signal to [0, 1] following the equation below:

$$signal_{normalized} = \frac{signal - \min(signal)}{\max(signal) - \min(signal)} \quad (1)$$

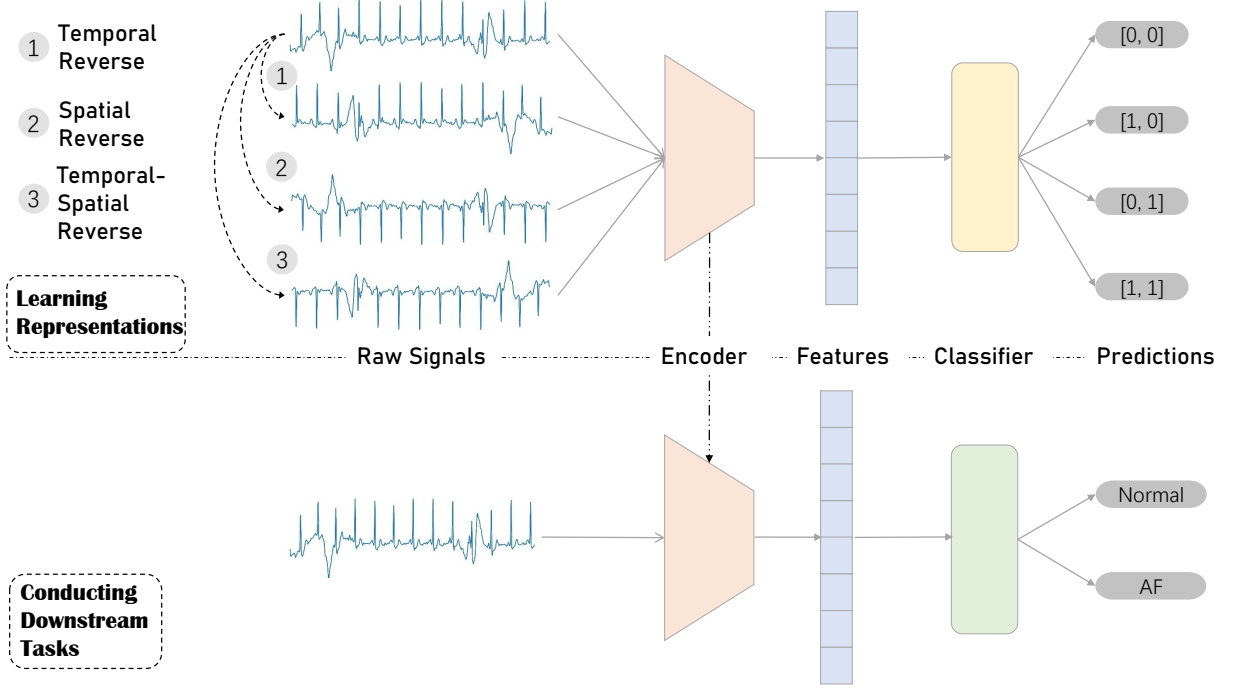


Figure 1: Overview of the two-stage framework with our method. The encoder is first trained in the stage of learning representations, and then transferred to conduct the downstream tasks.

Type	# of recordings	Time length (s)				
		Mean	SD	Max	Median	Min
Normal	5154	31.9	10.0	61.0	30	9.0
AF	771	31.6	12.5	60	30	10.0

Table 1: Overview of our adopted data. SD means standard deviation.

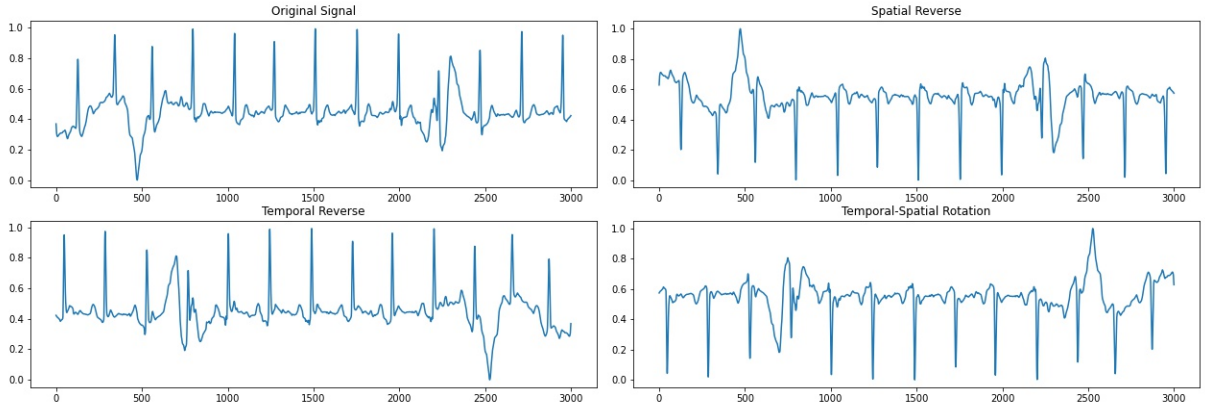


Figure 2: Original ECG segment and three types of reversed segments.

### 2.2. Overall framework for learning representations and conducting downstream tasks

The overall two-stage framework is shown in Figure 1. The first stage is for learning representations that is based on our temporal-spatial (T-S) reverse detection method. The representational model consists of two parts: encoder and classifier. The encoder produces the representations, and classifier is for conducting the classification (T-S reverse detection) task during the learning process. After the learning is finished, the trained encoder is transferred to the second stage for various downstream tasks. We only show our experimental AF detection downstream task in Figure 1.

### 2.3. Data manipulations for T-S reverse detection

To apply the T-S reverse detection method, we need to augment data with three types of simple manipulations which include temporal reverse (flipping horizontally), spatial reverse (flipping vertically), and temporal-spatial reverse (flipping both horizontally and vertically). The examples of segments are illustrated in Figure 2.

The details of the reverse manipulations are listed as follows.

- **Temporal reverse:** we regard flipping horizontally as temporal reverse, because it changes the temporal information of original signals. We hope that by discriminating horizontally reversed signals from original signals, the model can learn sequential information of ECG signals. From Figure 2, we can see that horizontally reversed signals are relatively difficult to detect compared with vertical reverse discussed below. Consequently, we suppose detecting horizontal reverse can learn more details, especially the non-peak parts. We let

$$s'[i] = s[3000-i+1], i = 1, 2, \dots, 3000$$

where  $s$  is a 10-second segment and 3000 is the length of it.

- **Spatial reverse:** we see flipping vertically as a method changing the spatial information of original signals, so we call it spatial reverse. As shown in Figure 2, it is obvious that the vertical morphology, especially the peaks, changes a lot after vertical reverse. We aim to enable the model to “observe” the spatial difference, so that the model can capture the information on vertical direction of ECG signals. The implementation can be divided as 2 steps. We firstly multiply each value of signals by -1. Thus, all signals are vertically reversed, but are in a range of  $[-1, 0]$ . Secondly, we re-normalize the reversed signals following Equation 1. Thus, all signals are vertically reversed and moved to  $[0, 1]$ .
- **Temporal-Spatial reverse:** temporal-spatial reverse is a combination of temporal and spatial reverse. By performing temporal-spatial reverse, we can enlarge the amount of training data. In addition, these rotated signals can improve the difficulty of our classification task, thus can improve the discrimination ability of the model. When we perform temporal-spatial reverse, we only need to make a horizontal reverse on the vertically reversed segments.

By training the representational model to detect the four classes of segments, we hope the model can learn both temporal and spatial information of ECG signals. In this way, we can obtain informative representations with unlabelled ECG signals, and use them for downstream tasks.

### 2.4. Interpretation of model

To better explain how the model detect temporal reverse and spatial reverse, we adopt layer-wise relevance propagation (LRP) [26] as the interpretation method. It has been employed in many physiology modeling tasks, such as a classification task on electroencephalography [27] and sleep stage classification on ECG [28].

LRP reveals how the model decides on the final prediction. It propagates backward from the outputs layer by layer, until it reaches the first layer. LRP can give the relevance scores ( $R$  scores) for all temporal points from the inputs. Each point corresponds to one  $R$  score which is considered as its contribution to the prediction of the model. The higher the  $R$  score is, the larger contribution the point provides to the final

prediction. Formally, we refer  $R_i^l$  as the  $R$  score of the  $i$ -th neuron in the  $l$ -th layer,  $R_i^{(1)}$  is  $R$  score of the  $i$ -th original temporal point.

We can write the prediction of the neural network as

$$f(x) = \sum_I R_i^{(1)} \quad (2)$$

Regarding each pair of consecutive layers, the relevance score of  $l + 1$  layer can be decomposed to

$$R_j^{(l+1)} = \sum_i R_{i \leftarrow j}^{(l,l+1)} \quad (3)$$

where  $R_j^{(l+1)}$  is the relevance score of the  $j$ -th neuron in the  $(l + 1)$  -th layer. Thus, we can obtain the relevance score of the  $l$ -th layer:

$$R_i^{(l)} = \sum_j R_{i \leftarrow j}^{(l,l+1)} \quad (4)$$

Here we define

$$R_{i \leftarrow j}^{(l,l+1)} = \frac{z_{ij}}{z_j + \epsilon \cdot \text{sign}(z_j)} R_j^{l+1} \quad (5)$$

where  $z_{ij} = w_{ij}x_i$ ,  $z_j = \sum_k z_{kj}$ ,  $w_{ij}$  is the weight between neurons  $i$  and  $j$ . . Thus, we obtain the final equation of computing  $R$  score:

$$R_i^{(l)} = \sum_j \frac{z_{ij}}{z_j + \epsilon \cdot \text{sign}(z_j)} R_j^{l+1} \quad (6)$$

We can use Equation 6 from prediction layer to the first layer (original input). Thus, we can obtain the  $R$  score of each temporal point.

### 3. Experiments

We conduct experiments to support our hypothesis that classifying reversed segments can help the model learn temporal and spatial information of ECGs.

#### 3.1. Model Implementation

Our model is modified based on a deep neural network backbone, a structurally designed [29] one-dimensional ResNeXt [30] model, that achieves state-of-the-art performance in ECG modeling [31, 32]. The employed network contains 32 layers in total and five stages, each of which contains two blocks. The basic block is a bottleneck architecture, consisting of a cascade of three convolutional layers, and blocks are residual-connected with shortcut connections [33, 34]. The first and third convolutional layers are convolutional layers with the kernel size set to 1, and the second is an aggregated convolutional layer [30] with the kernel size set to 16 and groups set to 16. The input length is downsampled to half in the second layer of the first block in the 2nd and 4th stages. The corresponding shortcut connections also use Max Pooling to downsample the identity. Before each convolutional layer, Swish activation [35] and dropout [36] are employed to achieve a nonlinear transformation. After seven stages, the last dimension is pooled by an average layer, and the prediction layer is a fully connected dense layer.

#### 3.2. T-S reverse detection

Our T-S reverse detection method is a classification task to classify the original, temporal reverse, spatial reverse and temporal-spatial reverse ECG segments. We label the segments using one-hot encoding. The original segments are labeled as  $[0, 0]$ , the temporal reverse segments are labeled as  $[0, 1]$ , the spatial reverse segments are labeled as  $[1, 0]$ , and the temporal-spatially reverse segments are labeled as  $[1, 1]$ .

### 3.3. Baselines

We conduct four baseline methods for comparison. The details of each baseline are listed as follows.

- **Random Projection (RP)**: We implement RP using the GaussianRandomProjection function in the scikit-learn library. RP reduces the dimension by mapping the original input space to the target space through a randomly generated matrix. The components of this random matrix are drawn from normal distribution  $\mathcal{N}(0, \frac{1}{dim})$ , where  $dim$  is the target dimension.
- **PCA**: The implementation of PCA is through the PCA function in the scikit-learn library. PCA can be used to decompose a high-dimensional dataset. High-dimensional data is projected to a set of successive orthogonal components that contribute most to the variance.
- **AE**: We conduct a simple implementation of AE using PyTorch. AE is composed of two parts: the encoder and the decoder. The encoder is to map the original input  $x$  in data space to  $z$  in feature space, and the decoder is to reproduce  $x'$  (a reconstruction of  $x$ ) by mapping  $z$  back to data space. AE is trained by minimizing the reconstruction loss:

$$\mathcal{L} = \sum_{i=1}^N (x_i - x'_i)^2 \quad (7)$$

where  $N$  is the dimension of original data. In our experiment, the encoder is a ResNet-18 network, and the decoder has the symmetric structure.

- **SimCLR [37]**: SimCLR is a contrastive learning method. We conduct two types of data augmentation methods on raw signals, which are permutation and adding noise. The same segments with two augmentation methods are seen as positive pairs, and any two different segments (with either same or different augmentation methods) are regarded as negative pairs. The loss function of each positive pair (i,j) is

$$\mathcal{L} = -\mathbb{E}\left[\frac{e^{\text{sim}(x_i, x_j)/\tau}}{\sum_{k \neq i} e^{\text{sim}(x_i, x_k)/\tau}}\right] \quad (8)$$

where  $\text{sim}(x, y)$  represents cosine similarity  $\frac{x^T \cdot y}{\|x\| \cdot \|y\|}$ . We construct  $N$  positive pairs from a batch of  $N$  segments. Then, we calculate the average of  $N$  losses and minimize it. The model trained with SimCLR has the same architecture as the model trained to detect T-S reverse.

### 3.4. Ablation Study

To evaluate the performance of temporal reverse detection and spatial reverse detection respectively, we conduct the ablation study as follows:

1. **Spatial reverse detection**: the spatial reverse only task is a binary classification task to distinguish spatially (vertically) reversed signals from original signals, without regarding temporal reverse. The original signals are labeled as 0, and spatially reversed signals are labeled as 1.
2. **Temporal reverse detection**: the temporal reverse only task is a binary classification task to detect the temporally (horizontally) reversed signals. The original signals are labeled as 0, and temporally reversed signals are labeled as 1.

### 3.5. Implementation details

Our experiment has two stages: learning representation (training encoding) on unlabeled data and finetuning on downstream AF detection task. The framework is shown in Figure 1.

In the first stage, we train encoders to reduce dimension of raw signals using our reverse detection method and the baseline methods. Three target dimension of encoders are chosen, which are 64, 128 and 256. While training each model, we perform a five-fold cross validation. Among the total data, 80 percents are used for training and validating (with 90% for training and 10% for validation), and the other 20 percents are for

testing. For our T-S reverse detection method, both ablation methods, SimCLR and AE, the batch size is set as 128 and initial learning rate is set as 0.01. We calculate the validation loss every 300 training steps. If the validation loss keeps increasing for 1500 successive steps (five times of validation), we halve the learning rate. We stop the training process when the learning rate is less than  $10^{-8}$ .

After training, we obtain 3 (number of target dimensions)  $\times$  5 (number of folds) encoders for each method.

Then, the trained encoders are transferred to the second stage to learn low-dimensional representations for downstream tasks. In the second stage, we conduct a AF/ non-AF classification task to evaluate the representations. We obtain the features encoded by trained encoders, and then apply a 2-layer fully-connected neural network (FNN) as the classifier on these features. We also use a five-fold cross validation in this stage, which is the same as the validation in the first stage.

The encoder trained using the  $i$ -th fold of the training data ( $D_{train}^i$ ) in the first stage produces low-dimensional representations  $R_{train}^i$  for  $D_{train}^i$  and  $R_{test}^i$  for the  $i$ -th fold of the test data. These generated representation  $R_{train}^i$  is used to train the classifier, and  $R_{test}^i$  is for evaluating the classifier. When training the classifier, we randomly select 1,000 samples per class from  $R_{train}^i$  rather than using all representations to mimic the scenario in the real world that labeled data is limited. For each  $i$ , we train and test the classifier 10 times to make the results more convinced.

All neural networks are implemented using PyTorch 1.7.1, and the 2-layer FNN is implemented using the MLPClassifier function in scikit-learn 1.0. All experiments are conducted on a server with 503 GB of RAM and an NVIDIA GeForce RTX 3090 GPU.

### 3.6. Model interpretation

We train a simple four-layer fully connected neural network to conduct LRP, because the aforementioned model is too complex to be interpreted with LRP. We aim to find out what the model focuses most on temporally reversed signals and spatially reversed signals respectively. As a result, we train two classification models with one for spatial reverse and the other for temporal reverse. We choose not to perform LRP on the model trained with our T-S method since the components blend together and we cannot tell how the  $R$  score is affected by each part. With LRP, we can visualize data points with different colors reflecting the values of the corresponding  $R$  scores.

## 4. Results

### 4.1. Evaluation metrics

The performance metrics we select to evaluate the performance of different combinations are the receiver operating characteristics area under the curve (AUC), accuracy, sensitivity and specificity. The calculation of the metrics are based on the following four terms.

- True positive (TP): number of samples labeled positive and predicted positive.
- True negative (TN): number of samples labeled negative and predicted negative.
- False positive (FP): number of samples labeled negative but predicted positive.
- False negative (FN): number of samples labeled positive but predicted negative.

The x-axis of the ROC curve is the false positive rate ( $\frac{FP}{FP+TN}$ ), and the y-axis is the true positive rate ( $\frac{TP}{TP+FN}$ ). The AUC can measure a binary classifier system as the discrimination threshold varies. It can also be regarded as the probability that a positive example ranks higher than a negative example [38]. Accuracy is the ratio of the number of truly classified samples to the number of samples:

$$\text{Accuracy} = \frac{TP+TN}{TP+TN+FP+FN} \quad (9)$$

Sensitivity (also called recall value) is the correct classification rate only regarding positive samples:

$$\text{Sensitivity} = \frac{\text{TP}}{\text{TP} + \text{FN}} \quad (10)$$

Specificity is the correct classification rate only regarding negative samples:

$$\text{Specificity} = \frac{\text{TN}}{\text{TN} + \text{FP}} \quad (11)$$

For accuracy, specificity and sensitivity, we obtain the threshold for classifying labels by maximizing the geometric mean value [39] as shown below:

$$\text{G-mean} = \sqrt{\text{Sensitivity} \times \text{Specificity}} \quad (12)$$

#### 4.2. Results of baselines and ablation study

In this section, we show the numeric results of experiment. Table 2 shows the four adopted metrics of baseline methods (the first four rows of each dim), our T-S reverse detection method (the last row of each dim) and the ablation experiments (the rest two rows of each dim). The results are obtained by finetuning using 2,000 ECG segments (1,000 segments per class).

As shown in Table 2, our T-S method outperforms baseline methods evidently in terms of all metrics. For example, in terms of AUC, T-S achieves 35.8%, 30.5% and 25.6% higher than the highest baseline when the dimensions of features are 64, 128 and 256 respectively. For other metrics, baselines get scores below 0.7 most of the time, but the value of T-S is always above 0.8.

With the ablation study, we see spatial reverse is a comparatively poor task for learning ECG representations with the four metrics obviously lower than other two pre-training tasks. Temporal reverse, on the other hand, contributes most to the performance. The performance of the temporal reverse detection is similar to T-S, and it sometimes even surpasses T-S on certain metrics.

We also compare the effect of the number of training data for the ablation methods and our T-S reverse detection method with a simple logistics regression classifier. In this experiment, we feed the classifier with different number of training data (50, 100, 200, 500, 1000 and 2000). Figure 3 shows the AUCs for different number of training data with feature dimension as 64, 128 and 256. The x-axis represents  $\log_2(\text{number of training data})$ . The results indicate that the spatial reverse detection is less effective than the temporal reverse detection and the the T-S reverse detection. In addition, because logistics regression can only regard the linear relationship of features, the downstream performance is not as high as using FNN classifier. In this case, T-S reverse detection behaves more prominent compared to the results shown in Table 2. When the number of training data is 2000, the T-S reverse detection achieves AUCs of 0.869, 0.878 and 0.875 for the three different dimensions, while the temporal reverse detection only gives 0.856, 0.862 and 0.845.

In addition, to evaluate our method for the situation when the training data is sufficient, we add a simple fully-connected layer to our encoder as the classifier and train it with ECG segments up to 20,000 (almost the entire training set). We compare the performance in terms of AUC between models trained from scratch without reverse tasks and the ones trained with the T-S task. From results shown in Table 3, we can see that pre-training with T-S reverse detection task helps improve the performance not only when the labeled data is limited but also when data is sufficient.

#### 4.3. Data distributions in feature spaces

After trained with temporal reverse classification and spatial reverse classification tasks, the models are able to project raw ECG segments into two feature spaces (we only regard the target dimension of 64). How data is distributed in each feature space contains much important to evaluate our methods.

In Figure 4, the first plot represents the feature space for the spatial reverse, and we can see that the yellow points corresponding to the ECG segments labelled with “AF” and blue points corresponding to samples labelled with “Normal” distribute evenly. It indicates that the model trained with spacial reverse



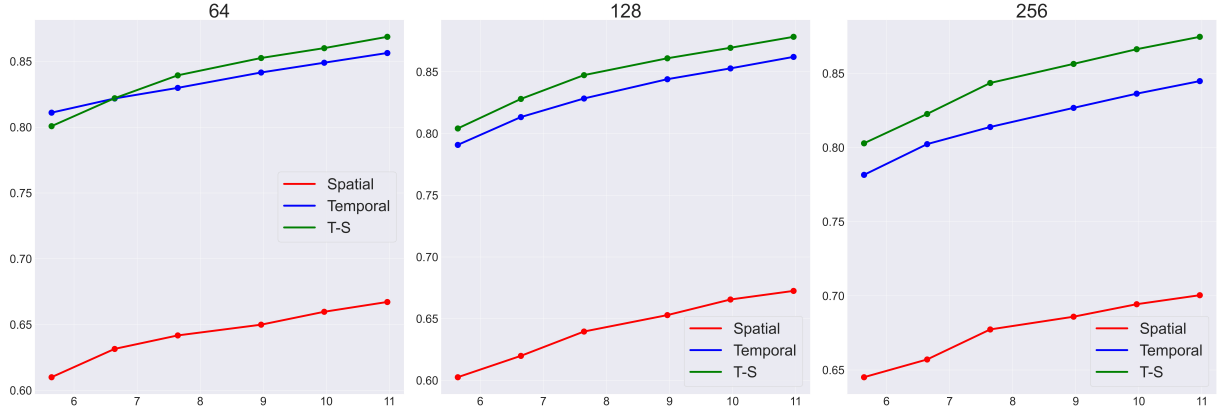


Figure 3: AUCs for different number of training data with feature dimension as 64, 128 and 256.

Dim	Methods	AUC	Sensitivity	Specificity	Accuracy
64	RP	$0.536 \pm 0.012$	$0.516 \pm 0.035$	$0.555 \pm 0.042$	$0.551 \pm 0.032$
	PCA	$0.597 \pm 0.009$	$0.567 \pm 0.032$	$0.584 \pm 0.030$	$0.582 \pm 0.023$
	AE	$0.658 \pm 0.015$	$0.594 \pm 0.032$	$0.652 \pm 0.028$	$0.645 \pm 0.022$
	SimCLR	$0.662 \pm 0.009$	$0.576 \pm 0.038$	$0.664 \pm 0.045$	$0.652 \pm 0.036$
	Spatial	$0.686 \pm 0.009$	$0.577 \pm 0.041$	$0.705 \pm 0.042$	$0.689 \pm 0.032$
	Temporal	$0.897 \pm 0.006$	<b><math>0.831 \pm 0.013</math></b>	$0.811 \pm 0.014$	$0.814 \pm 0.011$
	T-S	<b><math>0.899 \pm 0.006</math></b>	$0.804 \pm 0.013$	<b><math>0.832 \pm 0.013</math></b>	<b><math>0.829 \pm 0.010</math></b>
128	RP	$0.551 \pm 0.015$	$0.528 \pm 0.029$	$0.556 \pm 0.030$	$0.552 \pm 0.024$
	PCA	$0.586 \pm 0.009$	$0.556 \pm 0.021$	$0.581 \pm 0.023$	$0.577 \pm 0.018$
	AE	$0.662 \pm 0.017$	$0.594 \pm 0.037$	$0.660 \pm 0.040$	$0.651 \pm 0.032$
	SimCLR	$0.696 \pm 0.008$	$0.597 \pm 0.039$	$0.700 \pm 0.044$	$0.687 \pm 0.034$
	Spatial	$0.697 \pm 0.010$	$0.601 \pm 0.023$	$0.705 \pm 0.025$	$0.693 \pm 0.019$
	Temporal	$0.905 \pm 0.005$	$0.821 \pm 0.020$	$0.829 \pm 0.023$	$0.828 \pm 0.018$
	T-S	<b><math>0.908 \pm 0.005</math></b>	<b><math>0.822 \pm 0.018</math></b>	<b><math>0.836 \pm 0.015</math></b>	<b><math>0.834 \pm 0.011</math></b>
256	RP	$0.553 \pm 0.015$	$0.535 \pm 0.039$	$0.552 \pm 0.034$	$0.550 \pm 0.026$
	PCA	$0.554 \pm 0.012$	$0.521 \pm 0.027$	$0.566 \pm 0.025$	$0.560 \pm 0.019$
	AE	$0.655 \pm 0.013$	$0.591 \pm 0.034$	$0.647 \pm 0.029$	$0.651 \pm 0.022$
	SimCLR	$0.723 \pm 0.007$	$0.628 \pm 0.039$	$0.708 \pm 0.046$	$0.696 \pm 0.037$
	Spatial	$0.721 \pm 0.010$	$0.630 \pm 0.038$	$0.709 \pm 0.038$	$0.700 \pm 0.030$
	Temporal	$0.904 \pm 0.009$	$0.810 \pm 0.020$	<b><math>0.838 \pm 0.019</math></b>	<b><math>0.834 \pm 0.015</math></b>
	T-S	<b><math>0.908 \pm 0.008</math></b>	<b><math>0.830 \pm 0.025</math></b>	$0.831 \pm 0.023$	$0.831 \pm 0.017$

Table 2: The results of baselines and our methods training with 2,000 segments.

	50	100	200	500	1000	2000	20000
From scratch	0.662	0.735	0.836	0.917	0.932	0.933	0.963
T-S	0.873	0.906	0.936	0.956	0.966	0.973	0.981

Table 3: AUC on downstream task of models trained from scratch and trained from T-S.

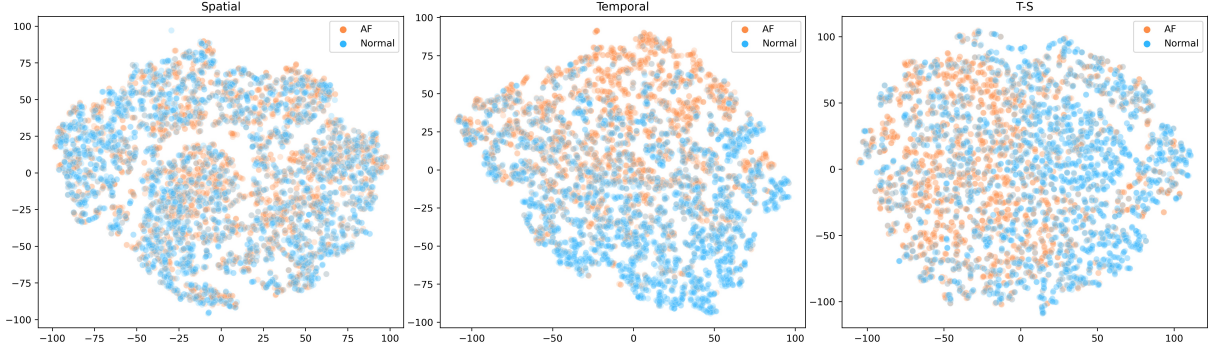


Figure 4: Data distributions in three feature spaces projected on 2-D planes.

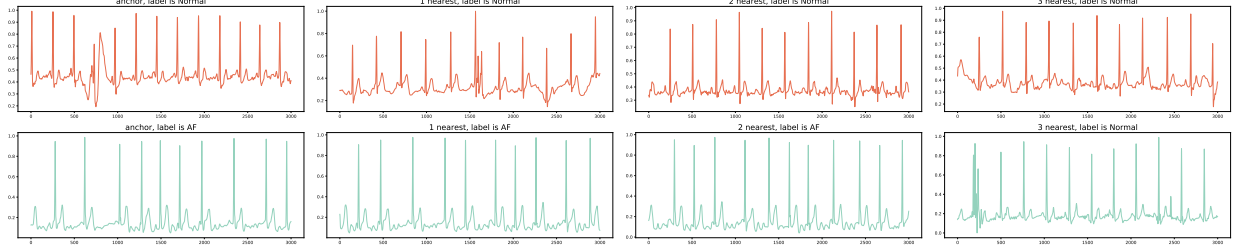


Figure 5: The 3-nearest segments of the anchor segments in the T-S feature space.

cannot distinguish between AF ECG segments and normal ECG segments. By contrast, the yellow “AF” points and the blue “Normal” points in the second and third plots are more discernible. From the second figure which represents the feature space for the temporal reverse, we can find more yellow points in the upper region and more blue points in the lower region. In the third figure that represents the feature space for the T-S reverse, yellow points tend to lie in the left and blue points tend to lie in the right. The plots illustrate that models trained to classify temporally reversed signals and classify T-S reversed signals have a better “understanding” about ECG that can provide representations containing more information to distinguish between AF and normal ECG segments.

We also conduct two case studies to demonstrate what the ECG segments that are close in the T-S feature space look like. We randomly select a “Normal” segment and a “AF” segments as two anchor segments. Then, we search for three nearest segments for each of them based on the euclidean distances of the outputs from the model that is trained with the T-S task. As shown in Figure 5, samples with same class labels (“AF” or “Normal”) are more likely to be closer in feature space.

#### 4.4. Results of model interpretation

As shown in Figure 6, we can see the two rows at the top have a more balanced color distribution, which means the different parts of ECG signals contribute more equally for the model trained with the temporal reverse task. On the other hand, the non-peak parts of signals are almost dark for the two rows at the bottom that correspond to the model trained with the spatial reverse task. It indicates the  $R$  scores of these parts are extremely small, thus the non-peak parts contribute little to final predictions.

## 5. Discussion

AF can cause two obvious changes on ECG signals. Firstly, P-waves may disappear in ECG signals of AF patients. At the same time, fibrillatory F-waves may appear in the TQ intervals. Secondly, patients suffered from AF have absolutely irregular ventricular rhythm. Thus, the RR intervals must have unequal lengths.

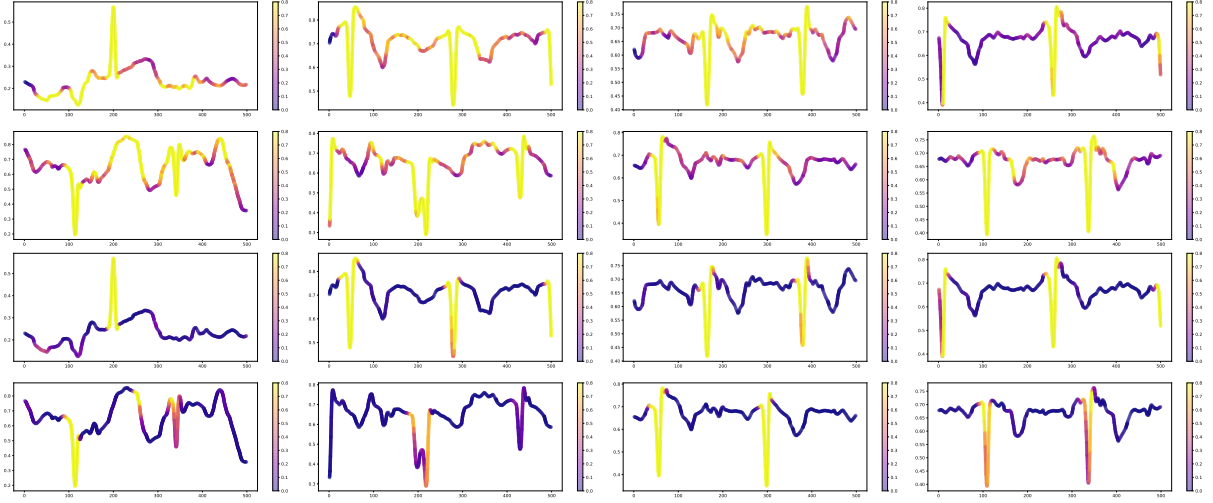


Figure 6: The results of model interpretation on 8 segments. The top 2 rows are from model trained by detecting temporal reverse, and the bottom 2 rows are from model trained by detecting spatial reverse.

Our spatial reverse detection and temporal reverse detection can correspond to these two changes well. The results shown in Table 2 indicate that detection of temporal reverse and spatial reverse both can help improve the performance on downstream tasks. Spatial reverse detection is helpful to the downstream AF classification task to some extent. This is mainly because the model trained by detecting spatial reverse can recognize the R peaks well and thus can the ventricular rhythm which is related to the RR intervals. As a result, it can notice irregular ventricular rhythm to some extent. In addition, irregular ventricular rhythm represents the abnormality on temporal dimension. Our temporal reverse detection aims to capture temporal information of ECGs. Thus, by detecting temporal reverse, the model can also classify normal and AF signals based on temporal difference.

We also explore the distribution in each feature space. As shown in Figure 5 and Figure 4, detection of temporal-spatial reverse and temporal reverse can help model project original segments to a feature space in which samples with same label are more likely to be closer. On the contrary, detecting spatial reverse shows little effect.

To understand why detection of temporal reverse is much more effective than spatial reverse, we use LRP to illustrate how the model learns from the original ECG signals under these two tasks. The R scores from LRP indicate that spatial reverse makes the model only focus on ECG peaks which proves our supposition that detection of spatial reverse is easily achieved by looking for the ECG peaks. It implies that detecting spatial reverse neglects some important spatial information such as P-waves. On the other hand, detection of temporal reverse makes the model pay attention to most temporal points along ECG signals which will facilitate the detection of AF.

Our detection of manipulated reverse signals can be easily performed in real-world scenario especially when labeled data is limited. The deep learning engineers can easily implement our method, and the performance on downstream tasks are no worse than sophisticated CL methods.

In terms of future work, we plan to test our method on more downstream tasks to see whether it is universally effective. In addition, the effectiveness of temporal reverse detection may be generalized to more methods. For example, we can construct a negative pair composed of an original signal and any temporally reversed signal. Thus, we can employ the pipeline of contrastive learning and see whether this is an appropriate way to construct pairs.

## 6. Conclusion

In this paper, we propose a simple but effective method learning ECG representations via detecting manipulated reverse on unlabeled data. By detecting three types of reverses, the model can learn effective representations for downstream tasks. The results show that our method outperforms other baselines substantially. In addition, we visualize the data in the feature space corresponding to the model trained with our method and conduct a case study to demonstrate that ECG segments with same class labels are close in the feature space. Results show that temporal reverse detection can help learn better representations for AF detection. Finally, we investigate the reason why temporal reverse reaches better performance than spatial reverse via the LRP interpretation method, and find out that temporal reverse makes the model consider a wider arrange along the ECG signals when making decisions. Our easily implemented but highly efficient method can provide a possible way to construct appropriate “pretext tasks” for self-supervised learning on ECG signals.

## Acknowledgment

This work was supported by the National Natural Science Foundation of China (No.62102008).

## References

- [1] S. J. Pan, Q. Yang, A survey on transfer learning, *IEEE Transactions on knowledge and data engineering* 22 (10) (2009) 1345–1359.
- [2] A. Krizhevsky, I. Sutskever, G. E. Hinton, Imagenet classification with deep convolutional neural networks, *Advances in neural information processing systems* 25 (2012) 1097–1105.
- [3] Y. Sun, S. Wang, Y. Li, S. Feng, X. Chen, H. Zhang, X. Tian, D. Zhu, H. Tian, H. Wu, Ernie: Enhanced representation through knowledge integration, *arXiv preprint arXiv:1904.09223* (2019).
- [4] D. E. Rumelhart, G. E. Hinton, R. J. Williams, Learning representations by back-propagating errors, *nature* 323 (6088) (1986) 533–536.
- [5] Y. LeCun, Y. Bengio, G. Hinton, Deep learning, *nature* 521 (7553) (2015) 436–444.
- [6] S. Hong, Y. Zhou, J. Shang, C. Xiao, J. Sun, Opportunities and challenges of deep learning methods for electrocardiogram data: A systematic review, *Computers in Biology and Medicine* 122 (2020) 103801.
- [7] J. Rahul, L. D. Sharma, Artificial intelligence-based approach for atrial fibrillation detection using normalised and short-duration time-frequency ecg, *Biomedical Signal Processing and Control* 71 (2022) 103270.
- [8] J. Han, G. Sun, X. Song, J. Zhao, J. Zhang, Y. Mao, Detecting ecg abnormalities using an ensemble framework enhanced by bayesian belief network, *Biomedical Signal Processing and Control* 72 (2022) 103320. doi:<https://doi.org/10.1016/j.bspc.2021.103320>. URL <https://www.sciencedirect.com/science/article/pii/S1746809421009174>
- [9] Ö. F. Ertuğrul, E. Acar, E. Aldemir, A. Öztekin, Automatic diagnosis of cardiovascular disorders by sub images of the ecg signal using multi-feature extraction methods and randomized neural network, *Biomedical Signal Processing and Control* 64 (2021) 102260.
- [10] Y. Tong, Y. Sun, P. Zhou, Y. Shen, H. Jiang, X. Sha, S. Chang, Locating abnormal heartbeats in ecg segments based on deep weakly supervised learning, *Biomedical Signal Processing and Control* 68 (2021) 102674.
- [11] R. Zhao, Y. Xia, Q. Wang, Dual-modal and multi-scale deep neural networks for sleep staging using eeg and ecg signals, *Biomedical Signal Processing and Control* 66 (2021) 102455.
- [12] J. Werth, M. Radha, P. Andriessen, R. M. Aarts, X. Long, Deep learning approach for ecg-based automatic sleep state classification in preterm infants, *Biomedical Signal Processing and Control* 56 (2020) 101663.
- [13] S. Hong, C. Wang, Z. Fu, Cardioid: Learning to identification from electrocardiogram data, *Neurocomputing* 412 (2020) 11–18.
- [14] Y. Zhang, Z. Zhao, Y. Deng, X. Zhang, Y. Zhang, Human identification driven by deep cnn and transfer learning based on multiview feature representations of ecg, *Biomedical Signal Processing and Control* 68 (2021) 102689. doi:<https://doi.org/10.1016/j.bspc.2021.102689>. URL <https://www.sciencedirect.com/science/article/pii/S174680942100286X>
- [15] A. Rasti-Meymandi, A. Ghaffari, A deep learning-based framework for ecg signal denoising based on stacked cardiac cycle tensor, *Biomedical Signal Processing and Control* 71 (2022) 103275.
- [16] H. Liu, Z. Zhao, Q. She, Self-supervised ecg pre-training, *Biomedical Signal Processing and Control* 70 (2021) 103010.
- [17] P. Sarkar, A. Etemad, Self-supervised learning for ecg-based emotion recognition, in: *ICASSP 2020-2020 IEEE International Conference on Acoustics, Speech and Signal Processing (ICASSP)*, IEEE, 2020, pp. 3217–3221.
- [18] D. Kiyasseh, T. Zhu, D. A. Clifton, Clocs: Contrastive learning of cardiac signals across space, time, and patients, in: *International Conference on Machine Learning*, PMLR, 2021, pp. 5606–5615.

- [19] X. Lan, D. Ng, S. Hong, M. Feng, Intra-inter subject self-supervised learning for multivariate cardiac signals, arXiv preprint arXiv:2109.08908 (2021).
- [20] S. Wold, K. Esbensen, P. Geladi, Principal component analysis, *Chemometrics and intelligent laboratory systems* 2 (1-3) (1987) 37–52.
- [21] H. Bourlard, Y. Kamp, Auto-association by multilayer perceptrons and singular value decomposition, *Biological cybernetics* 59 (4) (1988) 291–294.
- [22] E. Dasan, I. Panneerselvam, A novel dimensionality reduction approach for ecg signal via convolutional denoising autoencoder with lstm, *Biomedical Signal Processing and Control* 63 (2021) 102225.
- [23] M. Porumb, C. Griffen, J. Hattersley, L. Pecchia, Nocturnal low glucose detection in healthy elderly from one-lead ecg using convolutional denoising autoencoders, *Biomedical Signal Processing and Control* 62 (2020) 102054.
- [24] V. Kuznetsov, V. Moskalenko, D. Gribanov, N. Y. Zolotykh, Interpretable feature generation in ecg using a variational autoencoder, *Frontiers in Genetics* 12 (2021).
- [25] G. D. Clifford, C. Liu, B. Moody, L. H. Lehman, I. Silva, Q. Li, A. E. Johnson, R. G. Mark, Af classification from a short single lead ecg recording: The physionet/computing in cardiology challenge 2017, in: *2017 Computing in Cardiology (CinC)*, 2017, pp. 1–4. doi:10.22489/CinC.2017.065-469.
- [26] S. Bach, A. Binder, G. Montavon, F. Klauschen, K.-R. Müller, W. Samek, On pixel-wise explanations for non-linear classifier decisions by layer-wise relevance propagation, *PloS one* 10 (7) (2015) e0130140.
- [27] I. Sturm, S. Lapuschkin, W. Samek, K.-R. Müller, Interpretable deep neural networks for single-trial eeg classification, *Journal of neuroscience methods* 274 (2016) 141–145.
- [28] N. Banluesombatkul, P. Oupphaphan, P. Leelaarporn, P. Lakhan, B. Chaitusaney, N. Jaimchariya, E. Chuangsuwanich, W. Chen, H. Phan, N. Dilokthanakul, et al., Metasleeper: A pilot study on fast adaptation of bio-signals-based sleep stage classifier to new individual subject using meta-learning, *IEEE Journal of Biomedical and Health Informatics* (2020).
- [29] I. Radosavovic, R. P. Kosaraju, R. Girshick, K. He, P. Dollár, Designing network design spaces (2020). arXiv:2003.13678.
- [30] S. Xie, R. Girshick, P. Dollár, Z. Tu, K. He, Aggregated residual transformations for deep neural networks, in: *2017 IEEE Conference on Computer Vision and Pattern Recognition (CVPR)*, 2017, pp. 5987–5995. doi:10.1109/CVPR.2017.634.
- [31] S. Hong, Y. Zhou, M. Wu, J. Shang, Q. Wang, H. Li, J. Xie, Combining deep neural networks and engineered features for cardiac arrhythmia detection from ECG recordings, *Physiological Measurement* 40 (5) (2019) 054009. doi:10.1088/1361-6579/ab15a2.
- [32] S. Hong, Y. Xu, A. Khare, S. Priambada, K. Maher, A. Aljiffry, J. Sun, A. Tumanov, Holmes: Health online model ensemble serving for deep learning models in intensive care units, in: *Proceedings of the 26th ACM SIGKDD International Conference on Knowledge Discovery & Data Mining*, 2020, pp. 1614–1624.
- [33] K. He, X. Zhang, S. Ren, and J. Sun, Identity mappings in deep residual networks, in: *European conference on computer vision*, Springer, 2016, pp. 630–645.
- [34] K. He, X. Zhang, S. Ren, J. Sun, Deep residual learning for image recognition, in: *2016 IEEE Conference on Computer Vision and Pattern Recognition (CVPR)*, 2016, pp. 770–778. doi:10.1109/CVPR.2016.90.
- [35] P. Ramachandran, B. Zoph, Q. V. Le, Searching for activation functions, arXiv preprint arXiv:1710.05941 (2017).
- [36] N. Srivastava, G. Hinton, A. Krizhevsky, I. Sutskever, R. Salakhutdinov, Dropout: A simple way to prevent neural networks from overfitting, *Journal of Machine Learning Research* 15 (1) (2014) 1929–1958.
- [37] T. Chen, S. Kornblith, M. Norouzi, G. Hinton, A simple framework for contrastive learning of visual representations, in: *International conference on machine learning*, PMLR, 2020, pp. 1597–1607.
- [38] T. Fawcett, An introduction to roc analysis, *Pattern Recogn. Lett.* 27 (8) (2006) 861–874. doi:10.1016/j.patrec.2005.10.010.  
URL <https://doi.org/10.1016/j.patrec.2005.10.010>
- [39] M. Kubat, R. C. Holte, S. Matwin, Machine learning for the detection of oil spills in satellite radar images, *Machine Learning* 30 (2-3) (1998) 195–215.